

Signatures of Green's function zeros and their topology using impurity spectroscopy

Sayan Mitra,¹ Fang Xie,² Marek Kolmer,³ Qimiao Si,² and Chandan Setty^{†1,3}

¹*Department of Physics and Astronomy, Iowa State University, Ames, Iowa 50011, USA*

²*Department of Physics and Astronomy, Extreme Quantum Materials Alliance, Smalley-Curl Institute, Rice University, Houston, Texas 77005, USA*

³*Ames National Laboratory, U.S. Department of Energy, Ames, Iowa 50011, USA*

Topology without quasiparticles has emerged as a key framework for understanding Mott insulators, where Green's-function zeros encode nontrivial topological structure. Yet, experimental detection of these zeros represents a challenge. Using exact diagonalization of the one-dimensional Hubbard model with an impurity and Zeeman field, supported by exact analytic results, we show that Green's-function zeros manifest as an in-gap spectral weight in the unitary scattering regime. In this limit, we map the impurity problem onto a doped Mott insulator and identify the resulting in-gap state as a *zeron* excitation which is a *localized* doublon (holon) for an attractive (repulsive) potential. The zeron spectral weight and its associated zero vanish above a critical Zeeman field. Our results imply that Green's-function zeros have in fact already been observed in experiments, and establish impurity and magnetic-field tuning as practical tools for controlling their topology.

Introduction: The discovery and characterization of well-known topological phases and materials [1–5] rely on the existence of well-defined quasiparticles (QPs) [6]. However, strongly correlated systems, most notably Mott insulators [7, 8], often lack such a description: their single-particle Green's function develops *zeros* rather than poles [9], signaling QP loss. Recent theoretical work has therefore turned to the problem of defining topology in QP-absent regimes [10–12] by using Green's function zeros (GFZs) as the quantities of interest [11, 13–28].

Evidence from theoretical and numerical studies suggests that GFZs may carry a topological structure [11, 13–18, 20, 21, 23–28] and obey a form of bulk–boundary correspondence [15–17, 20, 24, 25, 28] similar to poles, but their physical meaning and experimental status remain unsettled. Crucially, unlike poles, GFZs leave no direct signature in standard spectroscopies, raising a fundamental question of whether and how they can be detected in real materials. The question of whether they are, in principle, measurable, was recently addressed by some of us, who showed that GFZs contribute to observable quantities in a gauge-invariant manner consistent with physical expectations [13]. Here we address the latter by showing that impurity spectroscopy provides a direct and experimentally accessible probe of GFZs and their topology through the emergence of in-gap states, which we term *zeron* excitations. In Mott insulators, these zeron correspond to highly localized doublons or holons. We further argue that zeron physics has in fact already been evidenced in prior experiments [29–48] in the context of doped Mott insulators. This identification is significant because it establishes a concrete link between theoretical descriptions of the topology of GFZs and their realization in measurable solid-state systems [19, 49].

Impurity Spectroscopy: Impurities serve as highly sensitive spectroscopic probes of electronic phases: properly tuned impurity potentials generate electron or hole bound states whose spectra encode the excitations of the surrounding host. It has been established that such impurity-induced features provide robust signatures

of metals, insulators, superconductors, and correlated phases [50]. We argue here that impurity spectroscopy also probes regimes of QP loss, thereby providing direct information about Green's function zeros. A useful starting point is the standard single-site T -matrix framework [50], which captures how a local impurity hybridizes with the excitations of an interacting host [51–56]. For an interacting system described by a Hamiltonian $H = H_I + H_{\text{imp}}$, where H_I denotes the translationally invariant Coulomb interacting Hamiltonian and H_{imp} represents a point-like (isotropic) impurity of strength V , the single-site T -matrix formalism [Supplemental Material (SM) [57] Sec. I] provides a controlled description of impurity scattering. Under simplifying assumptions of a local, momentum-independent impurity potential vertex, equivalently, s -wave scattering, the multiple-scattering processes generated by H_{imp} can be resummed to give

$$T(\omega) = \frac{V}{1 - V \sum_{\mathbf{k}} G^u(k, \omega)}, \quad (1)$$

where $G^u(k, \omega)$ is the interacting Green's function of the clean system (i.e., with $H_{\text{imp}} = 0$) derived typically under simplifying assumptions [51–56]. Obtaining $T(\omega)$ above requires resumming the Dyson series for the impurity Hamiltonian written in the fully interacting basis for a point impurity, and has been studied previously [51–56]. In conventional settings like ordinary metals or band insulators where $G^u(k, \omega)$ reduces to the non-interacting Green's function, the impurity-bound-state energy diverges in the unitary limit $V \rightarrow \infty$, with the scaling determined by dimensionality [see schematic Fig. 1(a)].

In sharp contrast, for a Mott insulator with GFZs, the T -matrix in the unitary limit ($V \rightarrow \infty$) yields at least one non-divergent in-gap impurity-induced bound state because $\sum_{\mathbf{k}} G^u(k, \omega) \rightarrow 0$ in the atomic limit [Sec. I.E of SM]. This behavior, characteristic of correlated systems lacking quasiparticles, is consistent with earlier theoretical approaches [56, 23] and is depicted in Fig. 1(b). We elucidate this physics using exact diagonalization of the one-dimensional Hubbard model with an onsite coulomb

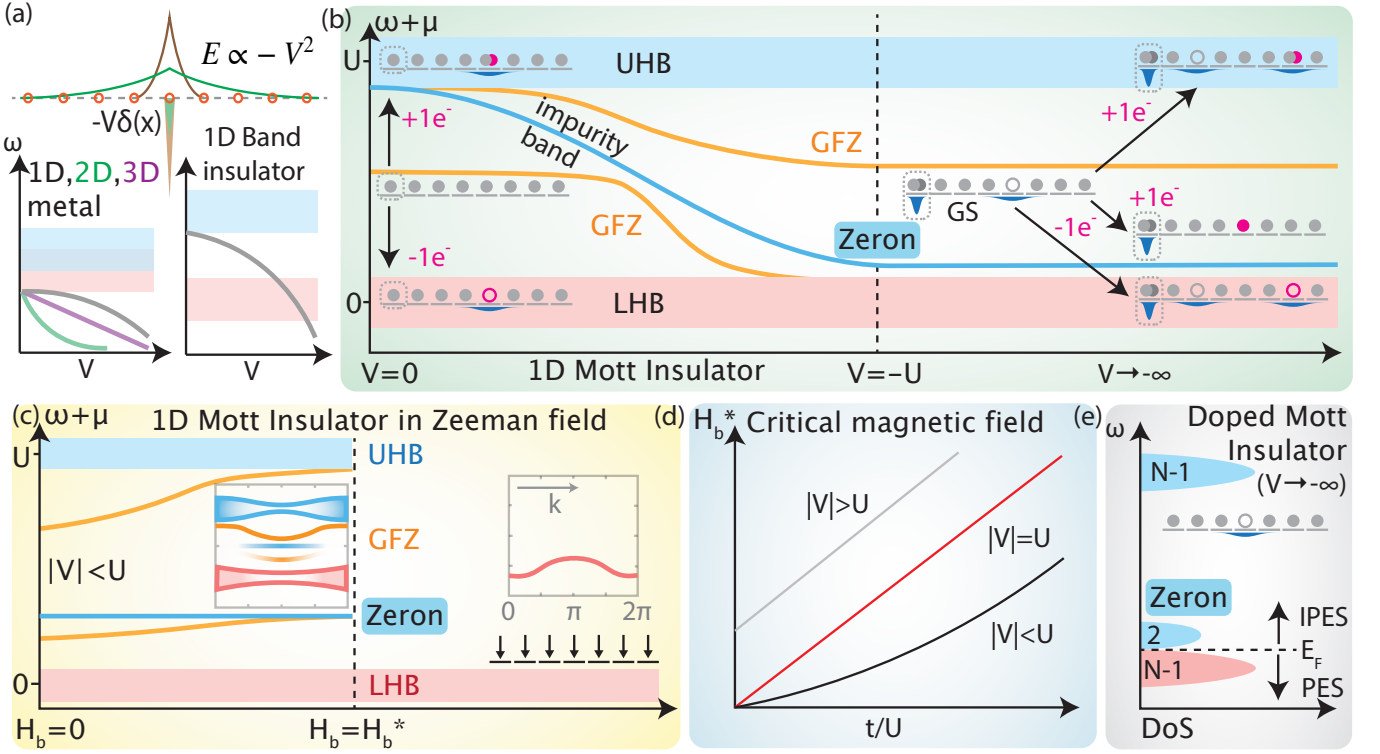


FIG. 1. Schematic figure illustrating the key results: (a) variation of the impurity-induced bound state energy for a Dirac delta impurity potential, in metals and in band insulators showing its divergence in the unitary ($V \rightarrow \infty$) limit. (b) In contrast for a Mott insulator with upper and lower Hubbard bands (UHB, LHB), and Green’s function zeros (GFZs), the impurity band asymptotes for $|V| > U$ due to the GFZs forming a *zeron* excitation. The disks and circles denote the content of initial and final eigenvectors leading to various observed spectral weights – the filled circles are electron and empty are holes. The arrows indicate single particle addition cc^\dagger and removal $c^\dagger c$ and the pink color indicates the added electron/hole; (c) If a Zeeman field is applied, the zeron and GFZs disappear for a critical field; the arrows indicate spin-down electrons and k is the wave-vector, inset figure showing the spectral function across the Brillouin zone. (d) For $|V| < U$, the critical field can be made arbitrarily small in the unitary limit ($t/U \rightarrow 0$), making it experimentally accessible; (e) Spectral function of a single-hole-doped Mott insulator with N sites, showing two in-gap zeron states above the LHB; in the unitary limit the impurity problem maps onto this doped system, identifying the zeron excitations as a manifestation of GFZs.

interaction U , and show that a Mott insulator hosting GFZs exhibits *saturation*, rather than divergence, of the impurity bound-state energy in the unitary scattering limit. This saturated in-gap spectral weight corresponds to the emergence of a zeron. The application of a Zeeman field H_b provides an additional diagnostic: above a critical field H_b^* , both the zeron spectral weight and the associated GFZ are quenched, as shown in Fig. 1(c). For $|V| \lesssim U$, H_b^* increases quadratically with the ratio t/U , but can be made experimentally accessible in the atomic limit $t/U \ll 1$ [Fig. 1(d)]. Figure 1(e) illustrates the appearance of in-gap spectral weight in the atomic limit of a Mott insulator doped with a single hole. We show that, in the unitary limit, attractive (repulsive) impurities map onto hole- (electron-) doped Mott insulators, producing an identical spectral weight and demonstrating generically that unitary scattering produces zeron excitations as a direct manifestation of GFZs. Our results imply that GFZs have in fact already been observed in experiments.

Model and Procedure: The Hubbard model Hamilto-

nian, with a single-site non-magnetic impurity V at site l and Zeeman field H_b is written as

$$H = \sum_{i,j} \sum_{\sigma} t_{i,j} c_{i,\sigma}^\dagger c_{j,\sigma} + U \sum_i n_{i,\uparrow} n_{i,\downarrow} + V (n_{l,\uparrow} + n_{l,\downarrow}) + H_b (n_{\uparrow} - n_{\downarrow}) \quad (2)$$

Here, $t_{i,j} = t$ is the nearest neighbor hopping, and $c_{i,\sigma}, n_{i,\sigma}$ are the annihilation and number operator at site i and spin σ . Exact Diagonalization (ED) is performed to evaluate the single particle Green’s function [See Secs. II and III of SM]. In the presence of an impurity, the Green’s function mixes momenta, even for a local isotropic potential; however, this mixing is not essential for the impurity properties of interest since the T -matrix itself is momentum independent for a local isotropic impurity. Further, our quantity of interest is the spectral function, as measured for example in photoemission, which requires only a single momentum label. The case of momentum mixing is discussed later and in SM. Therefore, we focus on the

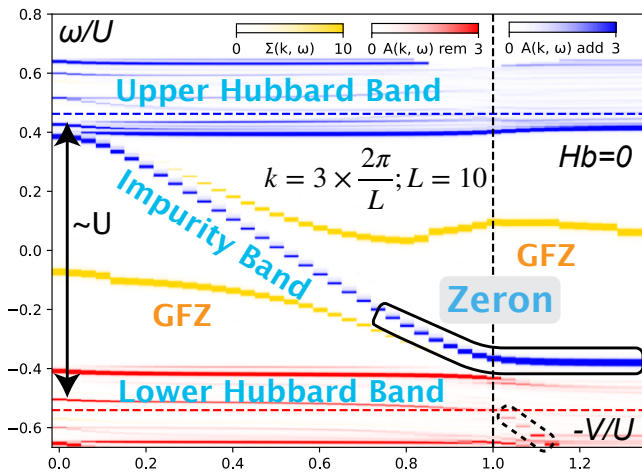


FIG. 2. Plot of $A_\sigma(k, \omega)$ and $\Sigma_\sigma(k, \omega)$ vs V for $\sigma = \downarrow$ or \uparrow , $k = 3/10 \times 2\pi$ (no Zeeman field), calculated for a 10-site lattice, highlighting the UHB, LHB, impurity band and GFZ, and also the saturation of the impurity band above the LHB. The bands are colored based on whether they originate from the particle addition or the removal term.

single-momentum Green's function, $\mathcal{G}_\sigma^u(k, \omega)$ given as

$$\mathcal{G}_\sigma^u(k, \omega) = \langle \psi_0^{(N)} | c_{k,\sigma}^\dagger \frac{1}{\omega - E_0^{(N)} + \hat{H}} c_{k,\sigma} | \psi_0^{(N)} \rangle + \langle \psi_0^{(N)} | c_{k,\sigma} \frac{1}{\omega + E_0^{(N)} - \hat{H}} c_{k,\sigma}^\dagger | \psi_0^{(N)} \rangle. \quad (3)$$

Here $E_0^{(N)}, |\psi_0^{(N)}\rangle$ are the N particle ground state energy and eigenvector. The first term in Eq. 3 is the single-particle removal term, which is measured via photoemission (ARPES), and the second term is the single-particle addition, measured using inverse photoemission Spectroscopy (IPES)[58]. The the experimentally measured spectral functions are $A_\sigma(k, \omega) = -\text{Im}[\mathcal{G}_\sigma^u(k, \omega)]$, and the GFZs are identified from numerical calculations using the self-energy $\Sigma_\sigma(k, \omega) = 1/G^0(k, \omega) - 1/\mathcal{G}_\sigma^u(k, \omega)$. The poles of $-\text{Im}[\Sigma](k, \omega)$ are where the GFZs are located. A broadening term $+i\eta$ with $\eta = 0.05$ is added to the denominator of Eq. 3. Out of the 52,920 eigenstates of half-filling ± 1 electrons on a 10-site lattice, only 1,000 states are used for the Green's function calculations. This number is large enough to study the range of energies around the Mott gap. By varying H_b and V , we calculate $\mathcal{G}_\sigma(k, \omega)$ and keep track of the poles and the zeros (GFZs) of the Green's function across the Brillouin Zone (BZ), i.e., $k = 0, 1 \dots L \cdot 2\pi/L$.

Results: In Fig. 2, the spectral functions $A_\sigma(k, \omega)$ and $\Sigma_\sigma(k, \omega)$ are calculated for a 10-site lattice and plotted for $k = 3 \times \frac{2\pi}{L}$. As described in Eq. 3, the Green's function is written as the sum of a particle addition and a particle removal term. The spin-up or down particle addition term, labeled as “ $A(k, \omega)$ add” is plotted in blue, and particle removal term, labeled as “ $A(k, \omega)$ rem”, is

plotted in red. At zero magnetic field ($H_b = 0$), as we introduce a small, non-zero V , an additional band, which we identify as the *impurity band* [Fig. 2], splits off from the UHB for $V < 0$ and LHB for $V > 0$. As $|V|$ is increased from 0 to U , the impurity band travels in the Mott gap, asymptoting near the LHB for $V \approx -U$ or the UHB for $V \approx U$, indicating an additional in-gap bound state, in the unitary limit. We will see below that this additional spectral weight corresponds to a highly localized doublon (holon) for an attractive (repulsive) potential. As discussed in the main text, we identify this excitation as the *zeron* that results from the presence of GFZs in the parent Mott insulator.

To understand the nature of the zeron excitation, we inspect the eigenvectors in large impurity limit. We observe that the ground state ψ_N^0 has a localized doublon in the impurity site and a holon delocalized on the non-impurity sites [Fig. 1(b) and SM Sec. IV]. In order to understand why the degeneracy in the UHB is broken for $|V| > U$, one can look at the single particle addition ground state $\psi_{(N+1)}^0$ and excited state $\psi_{(N+1)}^{\text{excited}}$, in particular the expectation value of the site-wise number operator. The ground state $\psi_{(N+1)}^0$ has a localized doublon without any delocalized holon, and the excited state $\psi_{(N+1)}^{\text{excited}}$ has a localized doublon, a delocalized holon and a delocalized doublon. These particle addition states lead to the zeron and the LHB respectively. For no impurity, $\psi_{(N+1)}^0$ and $\psi_{(N+1)}^{\text{excited}}$ are degenerate because there is no localized holon or doublon [SM Sec. IV]. The particle removal states $\psi_{(N-1)}$ around the Mott gap are still degenerate for any value of impurity. For $V \rightarrow \infty$, the impurity site has a localized holon [SM Sec. IV] and the degeneracy is broken in the LHB for the particle removal states. A key conclusion of our eigenstate analysis is that the impurity site effectively decouples from the system in

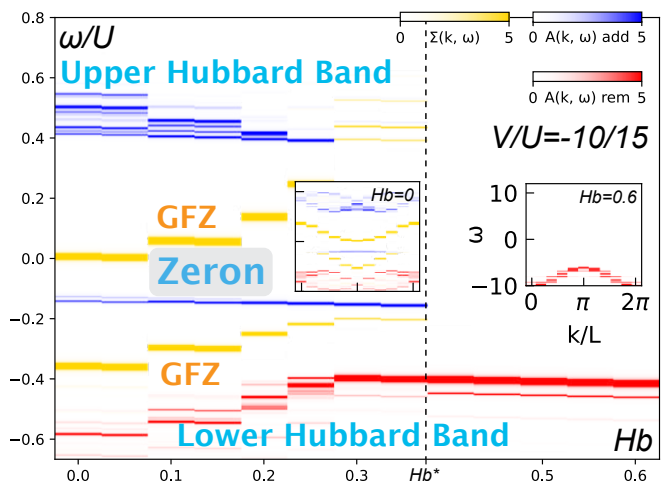


FIG. 3. Plot of $A_\sigma(k, \omega)$ and $\Sigma_\sigma(k, \omega)$ vs H_b for $\sigma = \downarrow$, $k = 5/10 \times 2\pi$, and $V/U = -10/15$. The UHB, LHB, and the impurity band are highlighted, showing the disappearance of impurity band for $H_b > H_b^*$. The inset plots are across the BZ for $H_b = 0$ and $H_b = 0.6 > H_b^*$.

the unitary limit, making it one-electron doped ($V \rightarrow \infty$) or one-hole doped ($V \rightarrow -\infty$) [SM Sec. IV]. Thus the analytic behavior of the Hubbard model with large on-site potential can be mapped to doping a Mott insulator.

The latter has been extensively investigated previously and an exact analytical treatment in the atomic limit is given in Refs. [7, 8, 59]. In the one-hole doped case, the missing electron shifts spectral weight between the lower and upper Hubbard bands while preserving the total of two states per site. The doped hole removes one state from the UHB and adds one to the LHB so that their combined weight remains fixed, and the empty impurity site contributes two low-energy addition states (spin up or spin down) inside the Mott gap, as shown in Fig. 1(e). Consequently, the impurity-induced in-gap band saturates at exactly the same total in-gap spectral weight as expected for a doped Mott insulator, providing a simple counting picture for the impurity-doped system [8, 59]. Hence, we conclude that the in-gap spectral weight for doped Mott insulator can be interpreted as a zeron for Hubbard model with a potential impurity. In contrast, for a band insulator where no GFZ occurs, a mid-band is seen for non-zero V , but it does not asymptote within the gap. By removing Coulomb interaction, $U = 0$, one can also study a single band metal, in which case also no GFZs or zeron are observed [See SM Sec. V].

We now study the effect of a Zeeman field by varying the H_b term in the Hamiltonian (Eq. 2). For no impurity ($V = 0$), as H_b is increased from zero, the system gets polarized until at a critical H_b , herein referred to as H_b^* , the system gets fully polarized $\langle S_z \rangle = -L/2$. Numerically, H_b^* is obtained where the $\langle S_z \rangle = -L/2$ ground state energy crosses the $\langle S_z \rangle = -L/2 + 1$ ground state energy [See SM Sec. VI.B]. For $H_b > H_b^* > 0$, the system is fully polarized with spin-down electrons, and with spin-up electrons for $H_b < H_b^* < 0$ [See SM Sec. VI.A.C]. In this fully polarized limit the model is exactly solvable and has been extensively studied, including within dynamical mean-field theory [60]. Because the half-filled system contains electrons of a single spin species, there are no available states to add an electron of the same spin, and the UHB and GFZ are therefore expected to disappear. As a result, the zeron excitation is also ex-

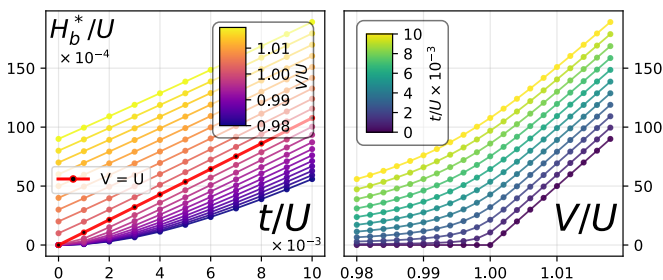


FIG. 4. H_b^*/U vs (a) t/U and (b) V/U in the unitarity limit ($U/t \rightarrow \infty$). H_b^* is parabolic in t for $V < U$ and linear for $V > U$. In the unitarity limit, H_b^* is nearly constant close to zero for $V < U$ and linear for $V > U$.

pected to be quenched in the fully polarized phase. This behavior is also expected for non-zero V and $|V| < U$. In Fig. 3, the spin down spectral functions are plotted vs H_b in the center of BZ for $V/U = 10/15$ [see SM Sec. VI B for a discussion on spin asymmetry]. Notice the disappearance of the zeron, UHB, and GFZ for $H_b > H_b^*$. The inset panels show the spectral functions across BZ for $H_b = 0$ and $H_b = 0.6 > H_b^*$. Detailed studies on the stability of GFZs to interactions appear in Refs. [61–64].

We now show that H_b^* may be experimentally accessible in certain limiting cases [see also SM Sec. VI.C]. Fig. 4(a) shows H_b^*/U versus t/U for different V , illustrating that for $V \lesssim U$ the critical field is quadratic in t/U and vanishes in the atomic limit $t/U \rightarrow 0$. The dependence of H_b^* with t/U crosses over from quadratic to linear as V increases, and for $V \gtrsim U$, H_b^* becomes linear. In this regime, full spin polarization requires the Zeeman field to energetically decouple the doublon localized at the impurity site, whose potential energy is set by V , leading to the observed linear scaling of H_b^* [see SM Sec. VI.C]. Fig. 4(b) plots H_b^*/U as a function of V/U for several values of t/U ; notably, in the atomic limit H_b^* can be made arbitrarily small for $V \lesssim U$. Finally, we note that for inelastic scattering, characterized by $A_\sigma(k, k' \neq k, \omega)$ [see SM Sec. VIII], the upper and lower Hubbard bands are strongly suppressed, while the zeron contribution remains pronounced for $k \approx k'$. To realize a minimal setup to diagnose the topology of GFZs, Fig. 5 illustrates the interacting topological systems with boundary GFZs. In the noninteracting model, the bulk is gapped while topological boundary modes reside at the edges without any GFZs. Upon introducing Coulomb interactions (ideally smaller than the bulk gap), the boundary modes gap out into GFZs pinned to the boundary, whereas the bulk remains free of GFZs. Consequently, impurities in the boundary (bulk) lead to occurrence (absence) of zeron. This behavior establishes how impurity response can offer a diagnostic of the topology of GFZs.

Materials and experimental considerations. As dis-

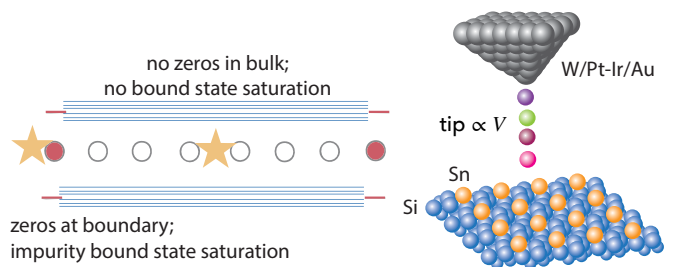


FIG. 5. Probing boundary GFZs: (Left) Projection of bulk-boundary states with impurity. As the bulk is an ordinary insulator without GFZs while the boundary has GFZs associated with interaction-gapped edge states, zeron occur only when the impurity is localized at the boundary. (Right) Proposed STM/STS experiment in Mott-insulating materials with engineered dopants added on Sn/Si(111) [65, 66], where the tip is used to tune the impurity potential.

cussed above, in the unitary limit of impurity scattering the problem of a potential impurity in a Mott insulator becomes equivalent to that of a doped Mott insulator. In this limit, several experiments have already reported the emergence of in-gap spectral weight—the very feature predicted by our theory. In the cuprate context, oxygen K-edge X-ray absorption spectroscopy on $\text{La}_{2-x}\text{Sr}_x\text{CuO}_{4+\delta}$ and $\text{YBa}_2\text{Cu}_3\text{O}_{6+x}$ demonstrates doping-dependent appearance of in-gap states [29, 30]. STM/STS on $\text{Ca}_2\text{CuO}_2\text{Cl}_2$ reveals particle-hole symmetric Hubbard bands and strongly localized in-gap states around intrinsic defects [31]. Controlled electron doping of $\text{Ca}_2\text{CuO}_2\text{Cl}_2$ by sub-monolayer Rb deposition further demonstrates progressive Mott-gap filling and emergent in-gap spectral weight [35], with related STM observations in $(\text{Ca},\text{Na})_2\text{CuO}_2\text{Cl}_2$ [36]. Momentum-resolved ARPES using sequential in-situ electron doping reveals spectral-weight transfer and the appearance of low-energy states in the Mott gap [37, 38]. Optical and infrared spectroscopy show doping-driven redistribution of spectral weight in $\text{La}_{2-x}\text{Sr}_x\text{CuO}_4$ [39–41] and in electron-doped $(\text{Sr}_{1-x}\text{La}_x)_3\text{Ir}_2\text{O}_7$ [42]. STEM-EELS on $\text{Nd}_{1-x}\text{Sr}_x\text{NiO}_2$ further reveals a reshaping of the Mott-Hubbard landscape with carrier addition [43]. Related impurity-induced in-gap states have also been observed in oxygen-deficient Sr_2IrO_4 [44, 45], in 1T-TaS₂ and related dichalcogenides [46], and in the hole-doped monolayer Sn/Si(111) system showing Motttness [65, 66]. This impurity or doping induced in-gap spectral weight provides support for zeron excitations.

What is missing, however, are experiments where the impurity strength is systematically tuned from weak to unitary scattering, and thereby track the evolution and saturation of the impurity-bound-state (zeron) energy as the unitary limit is approached. We therefore propose STM/STS experiments in which dilute, nominally nonmagnetic impurities—substitutional dopants, vacancies, or adatoms—are intentionally introduced into correlated insulators such as Sr_2IrO_4 , $\text{Ca}_2\text{CuO}_2\text{Cl}_2$, 1T-TaS₂, Sn/Si(111) or suitable pyrite and Kondo insulators. By imaging the local density of states around individual impurities while varying impurity species [Fig. 5(right)], local environments, or tip-induced potentials, one can follow the bound-state dispersion as the effective scattering strength is driven toward the Mott scale. The atomic manipulation capabilities of STM [67] further enable systematic construction of impurity configurations, allowing in-situ verification of the predicted saturation of the impurity band. Our theory predicts that, in the presence of GFZs, this impurity band approaches a finite zeron excitation energy rather than diverging, and that both the zeron band and the GFZ are suppressed above a critical magnetic field H_b^* , which lies within the field range of modern STM experiments.

Discussion and conclusions: Several points are in order. First, we stress that the GFZs studied here

are interaction-driven, arising from Coulomb correlations that generate zeros in the determinant of the Green’s function in a multi-orbital system. This is fundamentally distinct from the noninteracting, topology-induced zeros appearing in individual matrix elements in the orbital basis [68–71], which are not the focus of this work. Second, although the critical field H_b^* can be made arbitrarily small for $V/U < 1$ near the atomic limit, it rapidly becomes impractically large away from this regime as it scales with U . This motivates targeting f -electron systems and Kondo insulators, where H_b^* is more accessible and the unitary limit is easier to achieve. Finally, our results are consistent with Refs. [56,23] which report properties of in-gap impurity states in a Mott insulator within slave-rotor and Hubbard operator approaches.

To conclude, we have shown that GFZs in Mott insulators leave experimentally accessible signatures through impurity spectroscopy. Using exact diagonalization of the Hubbard model with a potential impurity and Zeeman field, supported by analytic arguments, we demonstrated that a GFZ inside the Mott gap produces a saturated impurity band in the unitary scattering limit that we term as a *zeron* excitation. In the Mott context, zeron are highly localized doublons (holons) nucleated by a strong attractive (repulsive) impurity potential. This is in sharp contrast to the divergent behavior expected in conventional band insulators and metals. By mapping the unitary impurity problem onto a doped Mott insulator, we identified zeron in well-known Mott insulators, implying that GFZs have in fact already been realized experimentally. We further showed that both the zeron and associated GFZs vanish above a critical Zeeman field, providing a tunable and falsifiable diagnostic of quasiparticle breakdown. Finally, we proposed a platform in which the impurity strength can be tuned toward the unitary limit, enabling direct observation of zeron and its magnetic-field control. Together, these results elevate impurity scattering to a quantitative experimental tool for detecting and manipulating topology beyond QPs.

Acknowledgements: We thank M. Tringides, R. Flint, W. Ding, P. Canfield, A. Kaminski and R. Prozorov for discussions. S.M and C.S are supported by Iowa State University start-up funds and Laboratory Directed Research and Development program at Ames Lab with the U.S. Department of Energy. Work at Rice has been supported by NSF Grant No. DMR-2220603 (F.X.), and by the Robert A. Welch Foundation Grant No. C-1411 and VBBF ONR-VB N00014-23-1-2870 (Q.S.). M.K. was supported by the DOE Early Career Research Program. Part of the research was performed at the Ames National Laboratory which is operated for the USDOE by Iowa State University under Contract No. DE-C02-07CH11358.

† Email for correspondence: csetty@iastate.edu

- [1] Xiao-Liang Qi and Shou-Cheng Zhang, “Topological insulators and superconductors,” *Reviews of modern physics* **83**, 1057–1110 (2011).
- [2] M Zahid Hasan and Charles L Kane, “Colloquium: topological insulators,” *Reviews of modern physics* **82**, 3045–3067 (2010).
- [3] Joel E Moore, “The birth of topological insulators,” *Nature* **464**, 194–198 (2010).
- [4] N Peter Armitage, Eugene J Mele, and Ashvin Vishwanath, “Weyl and dirac semimetals in three-dimensional solids,” *Reviews of Modern Physics* **90**, 015001 (2018).
- [5] Jennifer Cano and Barry Bradlyn, “Band representations and topological quantum chemistry,” *Annual Review of Condensed Matter Physics* **12**, 225–246 (2021).
- [6] Lev Davidovich Landau and Evgenii Mikhailovich Lifshitz, *Statistical Physics: Volume 5*, Vol. 5 (Elsevier, 2013).
- [7] Patrick A Lee, Naoto Nagaosa, and Xiao-Gang Wen, “Doping a mott insulator: Physics of high-temperature superconductivity,” *Reviews of modern physics* **78**, 17–85 (2006).
- [8] Philip Phillips, “Colloquium: Identifying the propagating charge modes in doped mott insulators,” *Reviews of Modern Physics* **82**, 1719–1742 (2010).
- [9] Aleksei Alekseevich Abrikosov, Lev Petrovich Gorkov, and Igor Ekhalieovich Dzyaloshinski, *Methods of quantum field theory in statistical physics* (Courier Corporation, 2012).
- [10] Haoyu Hu, Lei Chen, Chandan Setty, Mikel Garcia-Diez, Sarah E Grefe, Andrey Prokofiev, Stefan Kirchner, Maia G Vergniory, Silke Paschen, Jennifer Cano, *et al.*, “Topological semimetals without quasiparticles,” arXiv preprint arXiv:2110.06182 (2021).
- [11] Chandan Setty, Fang Xie, Shouvik Sur, Lei Chen, Silke Paschen, Maia G Vergniory, Jennifer Cano, and Qimiao Si, “Topological diagnosis of strongly correlated electron systems,” arXiv preprint arXiv:2311.12031 (2023).
- [12] Vladyslav Kozii and Liang Fu, “Non-hermitian topological theory of finite-lifetime quasiparticles: Prediction of bulk fermi arc due to exceptional point,” *Physical Review B* **109**, 235139 (2024).
- [13] Chandan Setty, Fang Xie, Shouvik Sur, Lei Chen, Maia G Vergniory, and Qimiao Si, “Electronic properties, correlated topology, and green’s function zeros,” *Physical Review Research* **6**, 033235 (2024).
- [14] Chandan Setty, Shouvik Sur, Lei Chen, Fang Xie, Haoyu Hu, Silke Paschen, Jennifer Cano, and Qimiao Si, “Symmetry constraints and spectral crossing in a mott insulator with green’s function zeros,” *Physical Review Research* **6**, L032018 (2024).
- [15] Steffen Bollmann, Chandan Setty, Urban FP Seifert, and Elio J König, “Topological green’s function zeros in an exactly solved model and beyond,” *Physical Review Letters* **133**, 136504 (2024).
- [16] Niklas Wagner, Lorenzo Crippa, Adriano Amaricci, Philipp Hansmann, Marcel Klett, EJ König, Thomas Schäfer, D Di Sante, Jennifer Cano, AJ Millis, *et al.*, “Mott insulators with boundary zeros,” *Nature Communications* **14**, 7531 (2023).
- [17] Niklas Wagner, Daniele Guerici, Andrew J Millis, and Giorgio Sangiovanni, “Edge zeros and boundary spinons in topological mott insulators,” *Physical Review Letters* **133**, 126504 (2024).
- [18] Lei Chen, Haoyu Hu, Maia G Vergniory, Jennifer Cano, and Qimiao Si, “Dirac zeros in an orbital selective mott phase: Green’s function berry curvature and flux quantization,” arXiv preprint arXiv:2401.12156 (2024).
- [19] Carl Lehmann, Lorenzo Crippa, Giorgio Sangiovanni, and Jan Carl Budich, “Probing green’s function zeros by co-tunneling through mott insulators,” arXiv preprint arXiv:2502.19479 (2025).
- [20] Lei Su and Ivar Martin, “Global anomalies of green’s function zeros,” arXiv preprint arXiv:2405.08093 (2024).
- [21] Andrea Blason and Michele Fabrizio, “Unified role of green’s function poles and zeros in correlated topological insulators,” *Physical Review B* **108**, 125115 (2023).
- [22] Emile Pangburn, Catherine Pépin, and Anurag Banerjee, “Topological charge excitations and green’s function zeros in paramagnetic mott insulators,” *Physical Review B* **112**, 085105 (2025).
- [23] Emile Pangburn, Anurag Banerjee, Catherine Pépin, and Cristina Bena, “Impurity-induced mott ring states and mott zeros ring states in the hubbard operator formalism,” *Physical Review B* **112**, 125157 (2025).
- [24] Victor Gurarie, “Single-particle green’s functions and interacting topological insulators,” *Physical Review B—Condensed Matter and Materials Physics* **83**, 085426 (2011).
- [25] Andrew M Essin and Victor Gurarie, “Bulk-boundary correspondence of topological insulators from their respective green’s functions,” *Physical Review B—Condensed Matter and Materials Physics* **84**, 125132 (2011).
- [26] Yi-Zhuang You, Yin-Chen He, Cenke Xu, and Ashvin Vishwanath, “Symmetric fermion mass generation as deconfined quantum criticality,” *Physical Review X* **8**, 011026 (2018).
- [27] Kevin Slagle, Yi-Zhuang You, and Cenke Xu, “Exotic quantum phase transitions of strongly interacting topological insulators,” *Physical Review B* **91**, 115121 (2015).
- [28] Grigory E Volovik, *The universe in a helium droplet*, Vol. 117 (OUP Oxford, 2003).
- [29] CT Chen, F Sette, Y Ma, MS Hybertsen, EB Stechel, WMC Foulkes, M Schuller, Sang-Wook Cheong, AS Cooper, LW Rupp Jr, *et al.*, “Electronic states in la 2- x sr x cuo 4+ δ probed by soft-x-ray absorption,” *Physical review letters* **66**, 104 (1991).
- [30] J-Y Lin, PR Lee, YT Liu, Chung-Yu Mou, Y-J Chen, KH Wu, CW Luo, JY Juang, TM Uen, JM Lee, *et al.*, “Dynamical spectral weight in yba .2 cu .3 o .y probed by x-ray absorption spectroscopy,” arXiv preprint arXiv:1009.2560 (2010).
- [31] Cun Ye, Peng Cai, Runze Yu, Xiaodong Zhou, Wei Ruan, Qingqing Liu, Changqing Jin, and Yayu Wang, “Visualizing the atomic-scale electronic structure of the ca2cuo2cl2 mott insulator,” *Nature communications* **4**, 1365 (2013).
- [32] Haiwei Li, Shusen Ye, Jianfa Zhao, Changqing Jin, and Yayu Wang, “Imaging the atomic-scale electronic states induced by a pair of hole dopants in ca2cuo2cl2 mott insulator,” *Science Bulletin* **66**, 1395–1400 (2021).

- [33] Peng Cai, Wei Ruan, Yingying Peng, Cun Ye, Xintong Li, Zhenqi Hao, Xingjiang Zhou, Dung-Hai Lee, and Yayu Wang, “Visualizing the evolution from the mott insulator to a charge-ordered insulator in lightly doped cuprates,” *Nature Physics* **12**, 1047–1051 (2016).
- [34] Xiaobo Ma, Guangwei Wang, Rui Liu, Tianye Yu, Yiran Peng, Pengyu Zheng, and Zhiping Yin, “Correlation-corrected band topology and topological surface states in iron-based superconductors,” *Physical Review B* **106**, 115114 (2022).
- [35] Han Li, Zhaohui Wang, Shengtai Fan, Huazhou Li, Huan Yang, and Haihu Wen, “Mott gap filling by doping electrons through depositing one sub-monolayer thin film of rb on $\text{ca}_2\text{cuo}_2\text{cl}_2$,” *Chinese Physics Letters* **41**, 057402 (2024).
- [36] Y Kohsaka, K Iwaya, S Satow, T Hanaguri, M Azuma, M Takano, and H Takagi, “Imaging nanoscale electronic inhomogeneity in the lightly doped mott insulator $\text{ca}_2\text{x n ax c u o}_2\text{cl}_2$,” *Physical review letters* **93**, 097004 (2004).
- [37] Cheng Hu, Jianfa Zhao, Qiang Gao, Hongtao Yan, Hongtao Rong, Jianwei Huang, Jing Liu, Yongqing Cai, Cong Li, Hao Chen, *et al.*, “Momentum-resolved visualization of electronic evolution in doping a mott insulator,” *Nature Communications* **12**, 1356 (2021).
- [38] A Damascelli, DH Lu, and Z-X Shen, “From mott insulator to overdoped superconductor: evolution of the electronic structure of cuprates studied by arpes,” *Journal of Electron Spectroscopy and Related Phenomena* **117**, 165–187 (2001).
- [39] S Uchida, T Ido, H Takagi, T Arima, Y Tokura, and S Tajima, “Optical spectra of $\text{la}_2\text{-x sr x cuo}_4$: Effect of carrier doping on the electronic structure of the cuo_2 plane,” *Physical Review B* **43**, 7942 (1991).
- [40] A Lucarelli, Stefano Lupi, Michele Ortolani, Paolo Calvani, P Maselli, M Capizzi, P Giura, H Eisaki, N Kikugawa, T Fujita, *et al.*, “Phase diagram of $\text{la}_2\text{-x sr x cuo}_4$ probed in the infared: Imprints of charge stripe excitations,” *Physical review letters* **90**, 037002 (2003).
- [41] T Katsufuji, Y Okimoto, and Y Tokura, “Spectral weight transfer of the optical conductivity in doped mott insulators,” *Physical review letters* **75**, 3497 (1995).
- [42] Gihyeon Ahn, SJ Song, T Hogan, SD Wilson, and SJ Moon, “Infrared spectroscopic evidences of strong electronic correlations in $(\text{sr}1\text{-x la x})\text{3ir}2\text{o}7$,” *Scientific reports* **6**, 32632 (2016).
- [43] Berit H Goodge, Danfeng Li, Kyuho Lee, Motoki Osada, Bai Yang Wang, George A Sawatzky, Harold Y Hwang, and Lena F Kourkoutis, “Doping evolution of the mott–hubbard landscape in infinite-layer nickelates,” *Proceedings of the National Academy of Sciences* **118**, e2007683118 (2021).
- [44] Zhixiang Sun, Jose M Guevara, Steffen Sykora, Ekaterina M Pärschke, Kaustuv Manna, Andrey Maljuk, Sabine Wurmehl, Jeroen Van Den Brink, Bernd Büchner, and Christian Hess, “Evidence for a percolative mott insulator–metal transition in doped sr_2ir_4 ,” *Physical Review Research* **3**, 023075 (2021).
- [45] Jixia Dai, Eduardo Calleja, Gang Cao, and Kyle McElroy, “Local density of states study of a spin-orbit-coupling induced mott insulator sr_2ir_4 ,” *Physical Review B* **90**, 041102 (2014).
- [46] Wenhao Zhang, Jingjing Gao, Li Cheng, Kunliang Bu, Zongxiu Wu, Ying Fei, Yuan Zheng, Li Wang, Fangsen Li, Xuan Luo, *et al.*, “Visualizing the evolution from mott insulator to anderson insulator in ti-doped 1 t-tas_2 ,” *npj Quantum Materials* **7**, 8 (2022).
- [47] Fangfei Ming, Steve Johnston, Daniel Mulugeta, Tyler S. Smith, Paolo Vilmercati, Geunseop Lee, Thomas A. Maier, Paul C. Snijders, and Hanno H. Weitering, “Realization of a hole-doped mott insulator on a triangular silicon lattice,” *Phys. Rev. Lett.* **119**, 266802 (2017).
- [48] Fangfei Ming, X Wu, C Chen, Kedong D Wang, Peizhi Mai, Thomas A Maier, J Strokoz, JWF Venderbos, Cesar González, Jose Ortega, *et al.*, “Evidence for chiral superconductivity on a silicon surface,” *Nature Physics* **19**, 500–506 (2023).
- [49] Ziren Xie, Amir Mirzanejad, and Lukas Muechler, “Strong correlations, green’s function zeros and topological transitions in orbital-symmetry-controlled chemical reactions,” *arXiv preprint arXiv:2506.18984* (2025).
- [50] Alexander V Balatsky, Ilya Vekhter, and Jian-Xin Zhu, “Impurity-induced states in conventional and unconventional superconductors,” *Reviews of Modern Physics* **78**, 373–433 (2006).
- [51] W Ziegler, D Poilblanc, R Preuss, W Hanke, and DJ Scalapino, “T-matrix formulation of impurity scattering in correlated systems,” *Physical Review B* **53**, 8704 (1996).
- [52] P Lederer and Marcelo Javier Rozenberg, “Impurity scattering in a strongly correlated host,” *Europhysics Letters* **81**, 67002 (2008).
- [53] H Alloul, J Bobroff, M Gabay, and PJ Hirschfeld, “Defects in correlated metals and superconductors,” *Reviews of Modern Physics* **81**, 45–108 (2009).
- [54] EA Nowadnick, B Moritz, and TP Devereaux, “Quasiparticle interference and the interplay between superconductivity and density wave order in the cuprates,” *Physical Review B—Condensed Matter and Materials Physics* **86**, 134509 (2012).
- [55] Miaomiao Zhao, Wei-Wei Yang, Hong-Gang Luo, and Yin Zhong, “Friedel oscillation in non-fermi liquid: lesson from exactly solvable hatsugai–kohmoto model,” *Journal of Physics: Condensed Matter* **35**, 495603 (2023).
- [56] Wenxin Ding and Qimiao Si, “Local density of states induced near impurities in mott insulators,” *Physical Review B* **110**, L081104 (2024).
- [57] “Supplemental material,” .
- [58] Andrea Damascelli, Zahid Hussain, and Zhi-Xun Shen, “Angle-resolved photoemission studies of the cuprate superconductors,” *Reviews of modern physics* **75**, 473 (2003).
- [59] M. B. J. Meinders, H. Eskes, and G. A. Sawatzky, “Spectral-weight transfer: Breakdown of low-energy-scale sum rules in correlated systems,” *Phys. Rev. B* **48**, 3916–3926 (1993).
- [60] P. J. H. Denteneer and R. T. Scalettar, “Interacting electrons in a two-dimensional disordered environment: Effect of a zeeman magnetic field,” *Phys. Rev. Lett.* **90**, 246401 (2003).
- [61] Chandan Setty, “Pairing instability on a luttinger surface: A non-fermi liquid to superconductor transition and its sachdev-ye-kitaev dual,” *Physical Review B* **101**, 184506 (2020).
- [62] Chandan Setty, “Superconductivity from luttinger surfaces: Emergent sachdev-ye-kitaev physics with infinite-body interactions,” *Physical Review B* **103**, 014501 (2021).

- [63] Chandan Setty, “Dilute magnetic moments in an exactly solvable interacting host,” arXiv preprint arXiv:2105.15205 (2021).
- [64] Edwin W Huang, Gabriele La Nave, and Philip W Phillips, “Discrete symmetry breaking defines the mott quartic fixed point,” *Nature Physics* **18**, 511–516 (2022).
- [65] Fangfei Ming, Steve Johnston, Daniel Mulugeta, Tyler S Smith, Paolo Vilmercati, Geunseop Lee, Thomas A Maier, Paul C Snijders, and Hanno H Weitering, “Realization of a hole-doped mott insulator on a triangular silicon lattice,” *Physical Review Letters* **119**, 266802 (2017).
- [66] Fangfei Ming, X Wu, C Chen, Kedong D Wang, Peizhi Mai, Thomas A Maier, J Strocoz, JWF Venderbos, Cesar González, Jose Ortega, *et al.*, “Evidence for chiral superconductivity on a silicon surface,” *Nature Physics* **19**, 500–506 (2023).
- [67] Wonhee Ko, Chuanxu Ma, Giang D Nguyen, Marek Kolmer, and An-Ping Li, “Atomic-scale manipulation and in situ characterization with scanning tunneling microscopy,” *Advanced Functional Materials* **29**, 1903770 (2019).
- [68] Takahiro Misawa and Youhei Yamaji, “Zeros of green functions in topological insulators,” *Physical Review Research* **4**, 023177 (2022).
- [69] Robert-Jan Slager, Louk Rademaker, Jan Zaanen, and Leon Balents, “Impurity-bound states and green’s function zeros as local signatures of topology,” *Physical Review B* **92**, 085126 (2015).
- [70] Raquel Queiroz, Roni Ilan, Zhida Song, B Andrei Bernevig, and Ady Stern, “Ring states in topological materials,” arXiv preprint arXiv:2406.03529 (2024).
- [71] Kai Chen and Pavan Hosur, “Robust boundary luttinger surfaces in topological band structures,” *Physical Review B* **111**, 125132 (2025).